# Active Control of an Axial Flow Compressor via Pulsed Air Injection

Raffaello D'Andrea*‡ raff@hot.caltech.edu
Robert L. Behnken†‡ behnken@indra.caltech.edu
Richard M. Murray‡ murray@indra.caltech.edu

Division of Engineering and Applied Science
California Institute of Technology
Pasadena, California 91125

CDS Technical Report CIT/CDS 95-029
Submitted, *ASME J. Turbomachinery*

**Abstract**

This paper presents the use of pulsed air injection to control the onset of rotating stall in a low-speed, axial flow compressor. By measuring the unsteady pressures near the rotor face, a control algorithm determines the magnitude and phase of the first mode of rotating stall and controls the injection of air in the front of the rotor face. Experimental results show that this technique slightly extends the stall point of the compressor and eliminates the hysteresis loop normally associated with rotating stall. A parametric study is used to determine the optimal control parameters for suppression of stall. Analytic results—using a low-dimensional model developed by Moore and Greitzer combined with an unsteady shift in the compressor characteristic to model the injectors—give further insights into the operation of the controller. Based on this model, we show that the behavior of the experiment can be explained as a change in the bifurcation behavior of the system under nonlinear feedback. A higher fidelity simulation model is then used to further verify some of the specific performance characteristics that are observed in experiments.

## Nomenclature

| | |
|---|---|
| $a, B, l_c, m, \lambda, \mu$ | Compression system geometric parameters, see [23] |
| $\alpha, \beta, \delta$ | Convenient functions of above geometric parameters, equation (5) |
| $a_i$ | Coefficients of polynomial fit of $\Psi_{\mathrm{cnom}}$, equation (3) |
| $c_i$ | Coefficients of polynomial fit of $\Psi_{\mathrm{cu}}$, equation (3) |
| $u_i$ | Air injection control parameter (distributed model) |
| $A$ | Amplitude of sinusoidal flow coefficient perturbation |
| $D_A, D_E$ | Matrices which depend on the above geometric parameters, see [20] |
| $J$ | $A^2$ |
| $G$ | Discrete Fourier Transform matrix |

*Author partially supported by NSERC.
†Author partially supported by an NSF Graduate Research Fellowship.
‡Funding for this research was provided in part by AFOSR grant F49620-95-1-0409.

| | |
|---|---|
| $T, S$ | Matrices which depend on the above geometric parameters, see [20] |
| $\gamma$ | Throttle coefficient |
| $\gamma^*$ | Value of $\gamma$ corresponding to the peak of $\Psi_{\mathrm{cnom}}$ |
| $\bar{\phi}$ | Annulus average flow coefficient |
| $\bar{\psi}$ | Annulus average pressure rise coefficient |
| $\xi$ | Dimensionless time |
| $\Psi_{\mathrm{c}}$ | Compressor characteristic, equation (2) |
| $\Psi_{\mathrm{cnom}}$ | Nominal compressor characteristic, equation (3) |
| $\Psi_{\mathrm{cu}}$ | Change in compressor characteristic due to air injection, equation (3) |
| $\Psi_{\mathrm{csh}}$ | Locally shifted compressor characteristic, equation (15) |
| `angle1` | Threshold angle for air injector 1 |
| `angle2` | Threshold angle for air injector 2 |
| `angle3` | Threshold angle for air injector 3 |
| `jeton` | Minimum pulse width (in servo loops) |
| `mag` | Magnitude of first mode stall cell (based on pressure measurements) |
| `phase` | Phase of the first mode stall cell (base on pressure measurements) |
| `threshold` | Threshold for stall detection |
| `window` | Angle window for stall detection |

# 1 Introduction

As gas turbine engines have become better understood and better designed, substantial performance increases between engine designs have become harder to achieve, especially with passive control methods. The presence of full authority digital engine controllers (FADECs) on modern gas turbines has enabled the use of active control to achieve additional performance enhancement. Virtually all modern aircraft engines rely on the use of FADECs for controlling engine operation, although the use of dynamic feedback to modify engine operation is relatively rudimentary.

One example of the use of active control to improve engine performance is the Performance Seeking Control (PSC) program at NASA Dryden Flight Research Center. The basic idea behind performance seeking control is to modulate the engine parameters to achieve optimal performance based on the current operating conditions. In simulation studies, Smith et al. [26] reported a 15% increase in thrust and 3% decrease in fuel consumption by the use of a controller which scheduled engine parameters for improved steady state operation. Subsonic flight tests at NASA Dryden Flight Research Center [10] validated the technique and showed a 1–2% decrease in fuel consumption during minimum fuel mode operation and measured thrust increases of up to 15% during maximum thrust mode.

Future applications of active control to jet engines will increasingly rely on the use of dynamic feedback to modify the dynamics of the engine and provide enhanced stability which is currently unachievable with passive methods. The development of so-called smart engines [25] is an area of intense research activity, both in academia and in industry. A major goal is the use of feedback controllers to reduce the effects of performance limiting instabilities that currently constrain the available power and efficiency of jet engines. In addition to technological advances, success in this area requires new techniques for modelling of jet engine dynamics for the purposes of control, as well as development and application of advanced control techniques capable of taking into account the high noise levels and nonlinear operating characteristics of aeroengines.

An initial step in the development of active control techniques for gas turbine engines is active control of the compressor core of the engine. Two of the main limiting factors in the performance

of compression systems are rotating stall and surge. Rotating stall refers to a dynamic instability that occurs when a non-axisymmetric flow pattern develops in the blade passages of a compressor stage and forces a drastic reduction in the performance of the compressor. This degradation in performance is usually unacceptable and must be avoided. Surge is a large amplitude, axisymmetric oscillation in the compressor which results from exciting unstable dynamics in the overall pumping system. While surge and stall are separate phenomenon, the presence of stall is a precursor to the onset of surge in many compressor systems. A more detailed description of these phenomena and their effects on overall performance can be found in the survey paper by Greitzer [12].

The goal of active control of stall and surge is to improve *operability* of the engine by allowing operation closer to the current stall line of the compressor. One of the significant features of high-performance axial-flow compressors is hysteresis in the performance of the compressor before and after rotating stall. As a consequence, if the operating point of a compressor momentarily crosses over the stall line due to a transient effect, the operating point of the compressor does not return to its original value, but rather to a much lower pressure/flow point. Using active control methods it is possible to modify the dynamics of the system such that hysteresis effects are either delayed or eliminated (depending on the approach used).

### Previous Work

Early work on rotating stall and surge concentrated on developing theoretical models which captured the main features of the two effects. In [11], Greitzer presented a 1D (axial) model which predicted the onset of surge using a single parameter, $B$. For large values of $B$ the pumping system exhibits surge while for small values it operates in rotating stall. More recent work by Moore and Greitzer [23] gives a refined model of rotating stall and surge which uses three coupled, nonlinear, partial differential equations to model the pressure and flow in a compressor system. The Moore-Greitzer model is the starting point for many of the current models used for rotating stall. In additional to fundamental modeling issues, there has also been work in studying the details of how stall occurs in experimental systems (see Day [8] for a recent survey). The detailed dynamics of stall and surge are not yet understood, but the basic mechanisms of stall and surge are fairly well classified and models which capture the main features of these instabilities are currently available in the literature.

Recent papers by Abed et al. [1] and McCaughan [21, 22] give a good overview of the basic analysis techniques which can be brought to bear. These papers analyze the global bifurcation behavior of the uncontrolled system and illuminate the nonlinear characteristics of the system which lead to instability as well as hysteresis. These techniques are particularly important in understanding the difference between improving operability of the engine and stabilization of the unstable dynamics.

Despite of the complexity of the dynamics of the system, experimental work has demonstrated that active control can be used to extend the operating point of the compressor past the normal stall limit. Results by Paduano et al. [24] showed a 20% decrease in mass flow for stall inception using actuated inlet guide vanes to generate an upstream vortical distortion. They used circumferential modes to model the compressor, actuators, and sensors and assumed a decoupled, linear model for the evolution of the modal coefficients. Day [7] used a similar technique with air injection as the actuation scheme and achieved approximately 5% extension in the stall point. Day also explored the use of air injection for destabilizing finite stall cells by injecting air in the jet nearest the stall cell. The control design was ad hoc, but gave good performance and did not rely on modal behavior.

More directly related to the approach pursued in this paper is the work of Gysling and Greitzer

on active stabilization using aeromechanical feedback [13, 14]. They used an array of 12 small reed valves upstream of the rotor to inject air based on the unsteady pressure exerted on the reed valve in the presence of rotating stall. By properly tuning the mechanical properties of the reed valve mechanism, rotating stall was stabilized past the normal stall point of the compressor. A modal analysis (in the circumferential variable) of the controller was used to validate the experimental results on an analytical model.

A somewhat different approach is the use of 1D actuation via bleed valves for control of rotating stall and surge. The controllers are based on a relatively complex 1D model of the compressor which captures the hysteresis and global dynamics of the system. The controllers change the nonlinear characteristics of the system so that surge does not occur and the change in operating point due to rotating stall is minimized. The approach used by Badmus et al. [3] used axisymmetric actuation (an outlet bleed valve) to eliminate the hysteresis effects of stall and also prevent surge without eliminating the stall cells *per se*. A theoretical description of this approach has been given by Liaw and Abed [18]. More recent experimental and numerical investigations of this technique can be found in [9].

### Overview of Paper

We depart from these previous studies in the sense that we make use of a small number of pulsed air injectors as our means of actuation. The motivation for using pulsed air injection, as opposed to the proportional injection studied by Day [7], is that pulsed injectors are a potentially more practical technology for implementation on real engines. For similar reasons, we have concentrated on the use of wall mounted static pressure sensors for detecting stall rather than using hot wire anemometers. Indeed, one of the goals of our work is to indicate to what extent air injection is a viable actuation technology for stabilization of rotating stall. A preliminary version of our experimental results appeared in [6] and extends the earlier work of Khalak and Murray [17].

In addition to providing detailed experimental results on the use of pulsed air injection for stabilization of rotating stall, we also present an analysis of our approach using the Moore-Greitzer formulation to construct a low-order nonlinear model of the dynamics in the presence of the controls. We make use of a shifted compressor characteristic to model the effect of the actuators, in a manner similar to that presented in the dissertation of Gysling [13]. The analysis supports the experimental results obtained on our compressor and gives further insight into the role of pulsed air injection in the stabilization process. An early version of the analytical results was reported in [5].

This paper is organized as follows. We begin with a description of the experimental setup in Section 2. The relevant characteristics of the compressor system are described, including the steady state performance characteristic of the compressor and the effects of continuous air injection on the steady state performance characteristic. In Section 3, experimental results are presented for a control law that extends the operating region of the compressor slightly and virtually eliminates the hysteresis loop. A detailed parametric study is presented which gives the optimal settings for various control parameters. Section 4 contains an investigation of the basic properties of the control law using the Moore-Greitzer model combined with compressor characteristic shifting to model air injection. We conclude with simulations studies in Section 5 using the higher fidelity distributed model of Mansoux et al. [20], which confirm the legitimacy of modeling the air injection as a local shift of the compressor characteristic. Section 6 summarizes the main conclusions and indicates several possible avenues of future research.

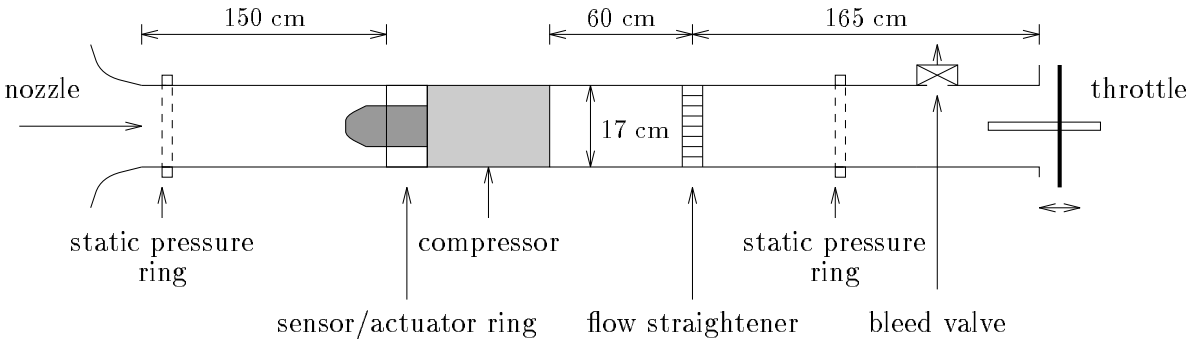


Figure 1: Caltech compressor rig.

## 2 Experimental Setup

In order to test the effects of air injection for stabilization of rotating stall, we have built a low-speed, axial flow compressor facility designed for use in validation of active control techniques. While this compressor is substantially simpler than a typical compressor in a gas turbine engine, it has many of the essential operating characteristics of high speed compressors and is ideally suited for implementation of active control techniques due to its size and ease of use.

The entire experimental setup is shown in Figure 1 and was designed and constructed in accordance with AMCA/ASHRE standards for measurement and calibration of compressors of this type [2]. The compressor is a 17 cm diameter, single stage, axial flow compressor. In addition to the compressor unit, the system consists of an inlet nozzle, adjustable downstream throttle, and an optional plenum. Sensors include a pair of static pressure rings on the inlet and outlet sides, a pitot measuring plane near the outlet, and an array of six static pressure transducers located in front of the compressor face. Actuation is achieved with a low-speed, electrically driven throttle at the outlet as well as a high response bleed which can be located either before or after the plenum and a set of three air injectors at the compressor face (described in more detail below).

For the experiments presented in this paper, the compressor was run at 6000 RPM, giving a peak head coefficient of 0.38 at a flow coefficient of 0.37. In physical units, this corresponds to 940 Pa at 0.19 $m^3/s$ . The high response bleed valve was only used to generate disturbances, and the optional plenum was only used in the experiments of Section 3.3. All sensors and actuators are interfaced to a PC-based real-time control computer running at a servo rate of 2000 loops per second.

The sensor ring shown in Figure 2 is located at the compressor inlet and used to measure the unsteady pressures upstream of the rotor. The ring has six pressure transducers equally spaced around the compressor circumference, approximately 5 cm (0.7 mean rotor radii) upstream of the rotor. These transducers have a resolution of approximately 1.2 Pa and a bandwidth of 1 kHz, and are low pass filtered at 500 Hz prior to sampling by a 12 bit A/D converter. The inlet and outlet static pressure rings shown in Figure 1 are instrumented with similar transducers, but are not filtered prior to sampling.

Three air injection actuators are also located on the sensor ring shown in Figure 2. The injectors are controlled by on/off solenoid valves which can be placed at a variety of (static) locations and orientations. The valves are actuated via custom overdriving circuitry interfaced directly to the computer, and are capable of a 50% duty cycle at up to 200 Hz. Hot-wire measurements were performed to determine the velocity profile of the air injection at the compressor face for the active control experiments outlined in Section 3. The injected air was found to disperse from 3 mm at

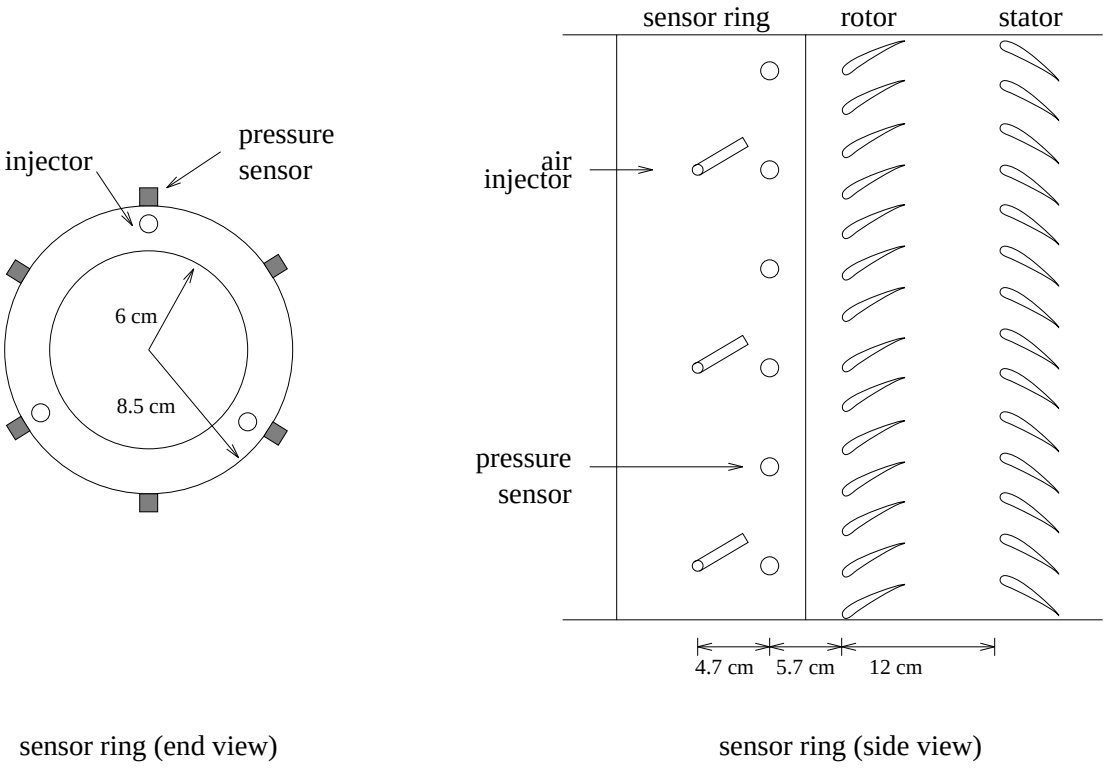


Figure 2: Sensor ring.

the exit of the injector to approximately 20 mm at the compressor face; this dispersion occurred over a distance of 9 cm (the distance between the exit of the air injector and the rotor face).

Three measures of control authority were calculated to characterize the air injectors; the mass flux, the momentum flux, and the energy flux. As a percentage of the mean values for the compressor operating at the peak of the compressor characteristic, the flow through each air injector on continuously contributed to 1.7% of the mass flux, 2.4% of the momentum flux, and 1.3% of the energy flux. Each of the control authority measures is thus small compared to the corresponding values for the compressor.

The dynamic behavior of the compressor system has many of the basic properties of high performance, axial flow compressors. The measured compressor characteristic is shown in Figure 3. The effect of rotating stall is clearly seen in the measured compressor characteristic. If the flow is decreased beyond the value at which the characteristic reaches its peak, the compressor enters rotating stall and operates at a much lower average pressure. Once in rotating stall the flow must be increased substantially before the system returns to the unstalled portion of the compressor characteristic.

The effects of the air injectors can be roughly characterized by their effect on the static compressor map. In [6], the effect of continuous air injection into the rotor face at different incident angles was investigated. The experimental results indicated that the compressor characteristic could be altered by air injection. In Figure 4, the shifted compressor characteristics are plotted for various incident angles. In these plots, the flow coefficient corresponds to the mass flow through the compressor (sum of the inlet mass flow plus the injected mass flow). Note that for positive angles (air injected into the blade rotation), the shifting of the characteristic is approximately the same, with the only difference being the stall inception point (as marked by circles).

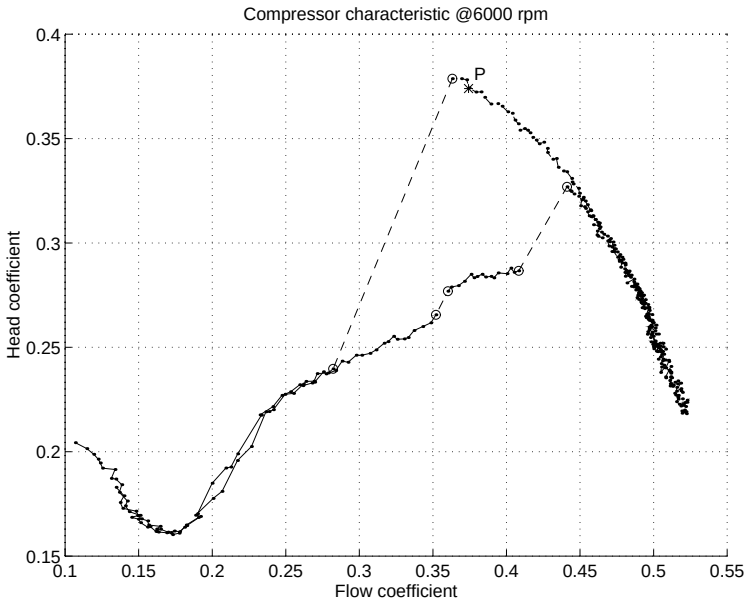


Figure 3: Fan characteristic for Able 29680 compressor at 6000 RPM. Dark lines indicate continuous changes in the operating point while lighter lines represent discontinuous changes. The circles mark the points of discontinuity. 'P' is the operating point for the parametric studies outlined in Section 3.

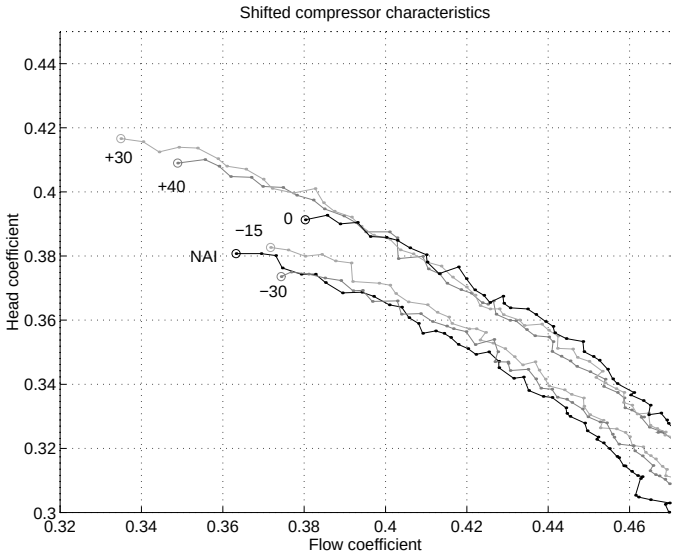


Figure 4: Compressor characteristics for various air injection angles. 'NAI' corresponds to the unactuated case (no air injection). The circles mark the peak operating point for each compressor characteristic.

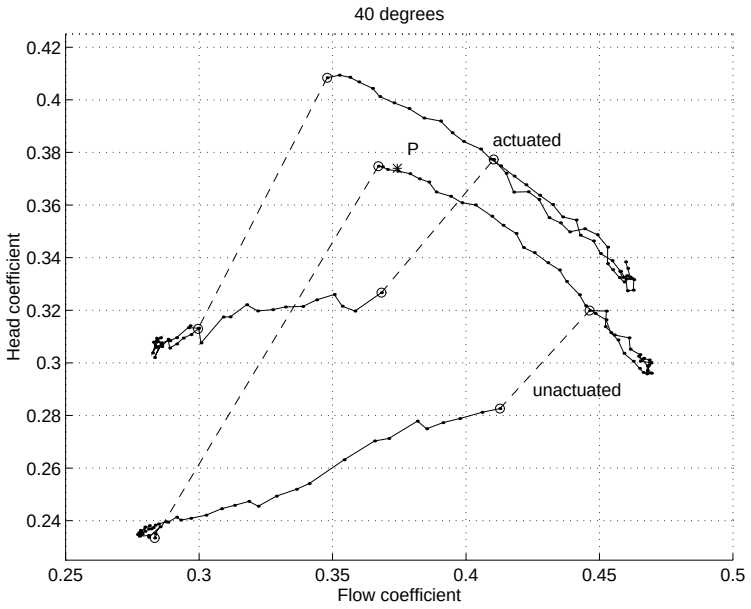


Figure 5: Compressor characteristic at air injection angle of 40 degrees. 'P' is the operating point for the parametric studies outlined in Section 3.

In Figure 5, the altered characteristic is plotted for an incident angle of 40 degrees, along with the unactuated characteristic for comparison purposes. This orientation was used for all the active control experiments in this paper.

# 3 Active Control

In this section, we present the experimental results on the use of air injection to control rotating stall. The effects of this control strategy on the surge dynamics are also explored.

## 3.1 Description of Control Algorithm

The basic strategy of the control algorithm is to sense the location and magnitude of the peak of the first mode component of a circumferential pressure disturbance and apply pulses of air based on the size and location of this first mode relative to the air injectors.

The plots in Figure 6 show the modal components of the pressure disturbance when a transition from unstalled to stalled behavior occurs. Since six equally spaced pressure transducers were used to measure the pressure disturbance, only the first two modes could be determined. As can be seen, the dominant mode is the first one. From the slope of the phase plots one can conclude that the first mode disturbance is rotating at a rate of approximately 65 Hz, while the second mode is rotating at approximately 130 Hz. This is consistent with a pressure disturbance rotating about the circumference of the compressor at a rate of 65 Hz. To ascertain that no significant aliasing was taking place due to the use of only six pressure transducers, time domain measurements were analyzed for each pressure transducer and the power spectrum determined. It was found that most of the signal power was contained in two bands centered around 65 Hz and 130 Hz. Assuming that the pressure disturbance is a traveling wave about the circumference of the compressor, this would

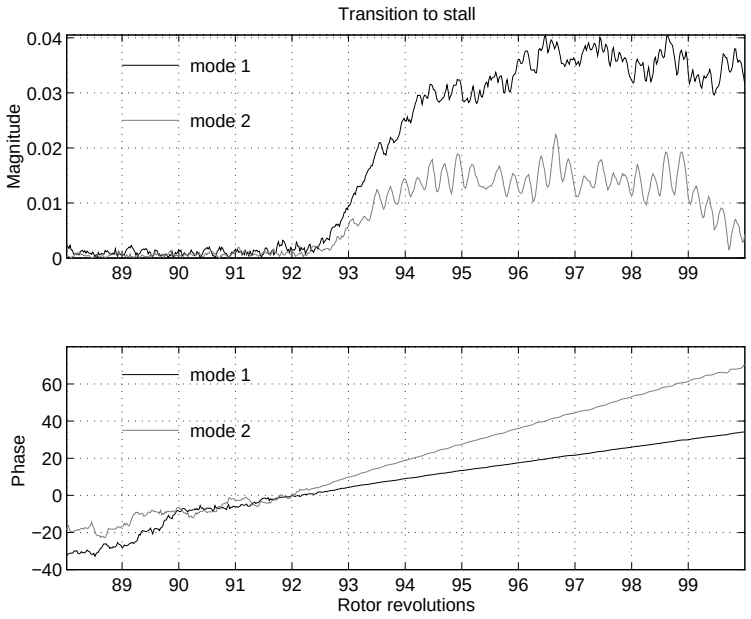


Figure 6: Transition to stall.

indicate that the third mode component is also negligible spatially about the circumference of the compressor.

The parameters used in the control algorithm are:

| | | | |
|---|---|---|---|
| `jeton` | minimum pulse width | `angle1` | threshold angle for air injector 1 |
| `threshold` | threshold for stall detection | `angle2` | threshold angle for air injector 2 |
| `window` | angle window for stall detection | `angle3` | threshold angle for air injector 3 |

The algorithm is shown in Figure 7, and behaves as follows. Each air injector is activated when the magnitude of the first mode is greater than `threshold` and the location of the peak of the first mode is within a pre-specified window (as determined by `angle` and `window`); once an air injector is activated, it remains activated for `jeton` number of servo-loops, irrespective of the magnitude `mag` and location `phase` of the first mode. Note that `phase` and `mag` refer to the phase and magnitude of the first Fourier coefficient, not the physical location and value of the peak pressure disturbance at the compressor face. In the case that the pressure disturbance is sinusoidal (which is a good approximation when fully stalled), `phase` and the physical location of the peak pressure disturbance differ by a constant, due to delays in the data acquisition stage. This delay was calculated to be 1.5 ms.

### 3.2 Parametric study

The controller parameters were varied in order to determine the optimal operating conditions for the controller, and to determine the effects on the closed loop behavior. The parameters varied were `jeton` and `angle1`, `angle2` and `angle3`. For this parametric study, the value of `threshold` was set to correspond to a head coefficient of 0.004 (10 Pa), and `window` was set to correspond to 25 degrees. The chosen value of `threshold` was slightly above that of the noise level, and thus allowed the control algorithm to sense a stall cell forming as quickly as possible. Assuming that

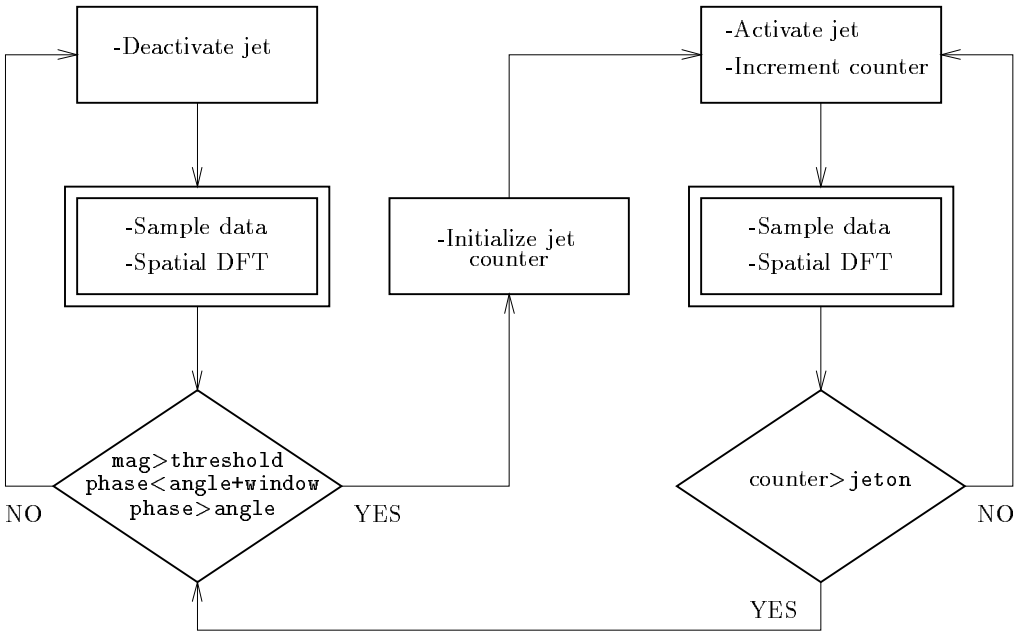


Figure 7: Control Algorithm. The above logic is repeated for each air injector. The double rectangle corresponds to the beginning of a servo loop, which occurs at a rate of 2000 loops per second.

the first mode rotates at a constant rate of 65 Hz, one servo loop corresponds to a rotation of 12 degrees. By setting `window` larger than this value, we are ensured that the peak of the stall cell disturbance will not be missed. On the other hand, the window should not be too large, to ensure that we do not have double activations (this is guaranteed by setting `window` $<$ 12`*jeton`), and to ensure that an air injector activates at the same time relative to the stall location (this might be a problem if the magnitude of the stall cell becomes greater than `threshold` near the end of an air injector's window). It was found experimentally that the value of `window` could be set in the range of 15 degrees to 90 degrees without changing the performance of the controller.

### Effect of activation angles

For a fixed value of `jeton`, a search was performed over the activation angle for each air injector to determine the optimal strategy. The compressor was operated at point $P$ in Figures 3 and 5. Parameters `angle1`, `angle2`, and `angle3` were each varied in 30 degree increments, from 0 to 330 degrees. Thus a total of 1,728 different controllers were tested for each value of `jeton`. For each of these settings, the control algorithm was operated for 16 seconds, and the average size of the stall cell and amount of time each air injector was on was recorded. A 0.1 second disturbance was generated every second via the high speed bleed valve to ensure that the compressor would stall.

The criterion used to determine the optimal setting for `angle1`, `angle2`, and `angle3` for a fixed `jeton` was the setting which yielded the lowest value for the average magnitude of the first mode (other criteria were also investigated, such as the total time that air injectors were on and the average pressure rise across the compressor, producing roughly the same results).

The results of this parametric study for `jeton` = 15 may be found in Figures 8 and 9. Referring to Figure 8, there are twelve separate plots, one for each setting of `angle1`. Dark areas correspond

to low average values for the first mode disturbance, while light areas correspond to large average values. From these plots, one may conclude that the optimal setting for `angle1`, `angle2`, and `angle3` is roughly $(90, 210, 330)$; the performance of the control algorithm was insensitive to simultaneous parameter deviations of up to 30 degrees from this optimal setting. The white asterisk in the plots corresponds to the optimal setting for `angle2` and `angle3`. The corresponding plots for `jeton` = 11, 13, 17 and 19 may be found in Figure 10. An alternate method of presenting the data for `jeton` = 15, which includes the magnitude of the first mode as a function of various parameter settings, may be found in Figure 9. A typical operation of the controller may be found in Figure 11.

### Effect of time delays

To fully understand the operation of the controller and properly interpret the experimental results, one must take into account the activation and deactivation delays of the air injectors. Using hot-wire measurements, the average activation delay for each injector was calculated to be 6.5 ms, while the deactivation delay was 4.5 ms. The activation delay corresponds to the total time it takes for the power of the injected air to reach 50% of its steady state value (at a distance of approximately 9 cm from the exit of the injector) from the time the injector was ordered to turn on; this delay takes into account the time required to open the solenoid valve and any delays in the air flow. Similarly for the deactivation delay.

Assuming a constant rotational speed of 65 Hz, we would like to determine what the relative position of the peak of the first mode disturbance is relative to the activation of each air injector. This is depicted in Figure 12 for `jeton` = 15 and air injector 1. The 90 degree rotation corresponds to the experimentally determined optimal lag; the 185 degree lag corresponds to the delay from sensing to actuation; the $-30$ degree rotation corresponds to the measured physical location where the injected air strikes the rotor face (recall that the air injectors were angled into the blade rotation). Thus air injector 1 activates approximately 55 degrees before the peak of the pressure disturbance and deactivates 70 degrees after the peak. Since the air injectors were physically spaced 120 degrees apart and the experimentally determined lags for `angle1`, `angle2`, and `angle3` were also spaced 120 degrees apart , the above argument holds for air injectors 2 and 3 as well. Thus the optimal setting for `angle1`, `angle2`, and `angle3` corresponds to a very intuitive control strategy: activate each air injector when the pressure is high and the flow is low. The above analysis can be performed for the other values of `jeton`, yielding similar results.

### Effect of pulse width

It was found that for values of `jeton` less than or equal to 9 and greater than or equal to 22 the compressor remained stalled all the time. Taking the activation and deactivation delays into account, a value of 9 corresponds to approximately 2.5 ms of on-time for each injector, or about 60 degrees when the disturbance rotates at 65 Hz. This amount of time apparently was not enough to bring the compressor out of stall.

A value of 22 for `jeton` corresponds to approximately 9 ms of on-time for each injector, or about 210 degrees at a rotation rate of 65 Hz. Thus for this value, an air injectors remain active even when the local flow is above the spatially averaged value through the compressor.

One can understand why there should exist an upper and a lower bound for values of `jeton` which eliminate stall through limiting arguments. Clearly for `jeton` = 0 (no control), the compressor will transition into stall. To understand what happens when `jeton` $= \infty$, one need only look at the plot of Figure 5; when operating near the stall point of the compressor, there are two possible operating points which the compressor may reach when all the air injectors are turned on. One

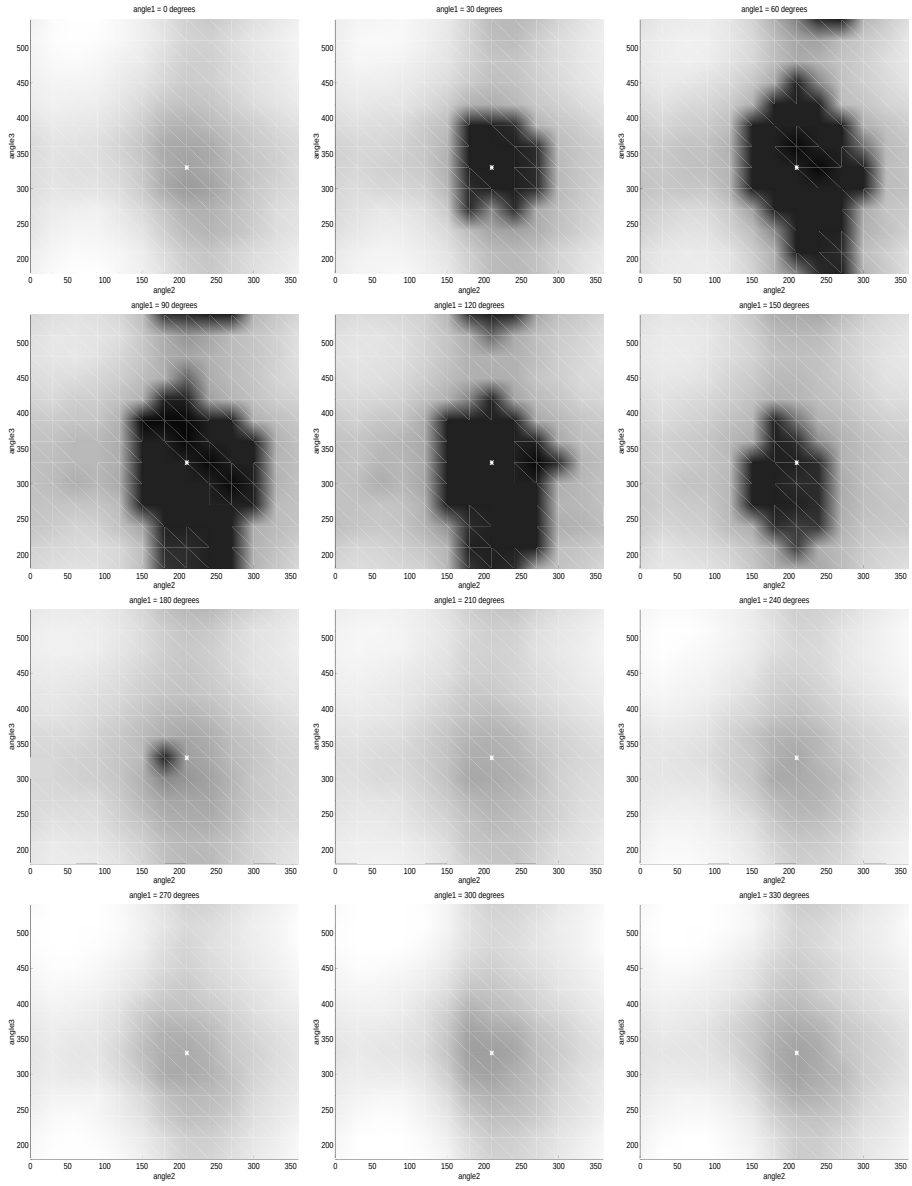


Figure 8: Parametric study, `jeton` = 15. Dark areas correspond to low average values for the first mode disturbance, light areas correspond to large average values. The white asterisk corresponds to the optimal setting for `angle2` and `angle3`, 210 and 330 degrees.

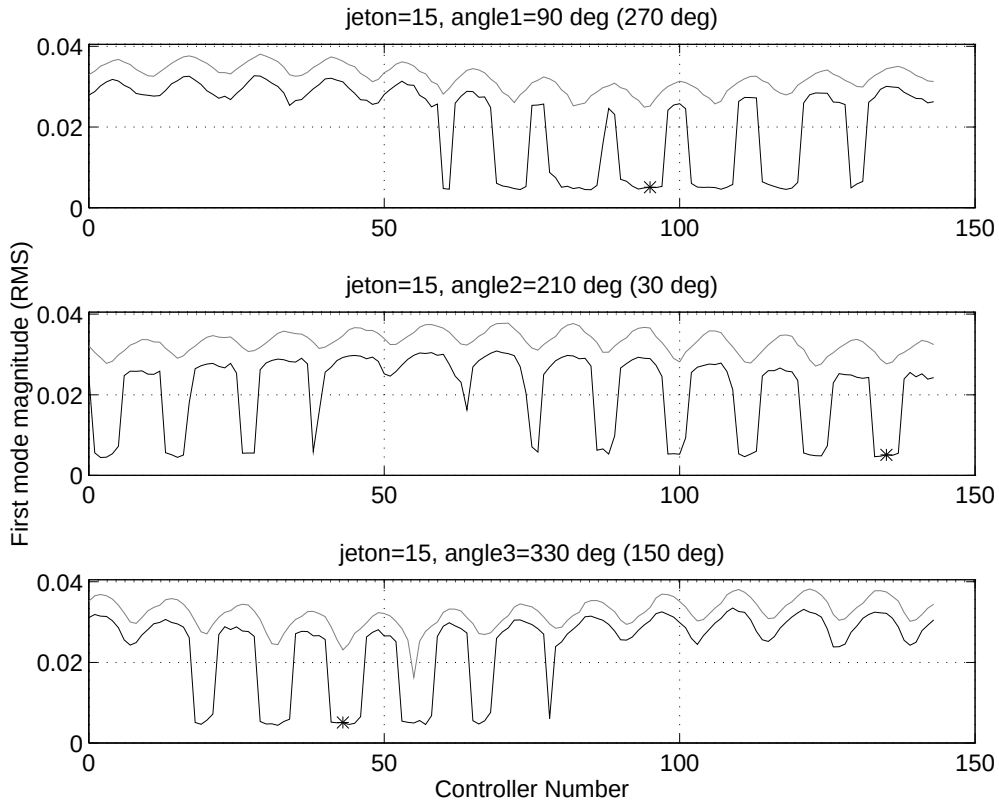


Figure 9: Parametric study, `jeton` = 15: RMS magnitude of first mode vs. controller number. The top plot corresponds to a fixed value for `angle1`, the second a fixed value for `angle2`, and the third a fixed value for `angle3`. The abscissa for the first plot is $12 * \texttt{angle2}/30 + \texttt{angle3}/30$, for the second plot $12 * \texttt{angle3}/30 + \texttt{angle1}/30$, and for the third plot $12 * \texttt{angle1}/30 + \texttt{angle2}/30$. The asterisk in each plot corresponds to the optimal setting. The dark curve for each plot corresponds to the optimal setting for that parameter, while the light curve corresponds to 180 degrees away from optimal (as per the bracketed value at the top of each plot).

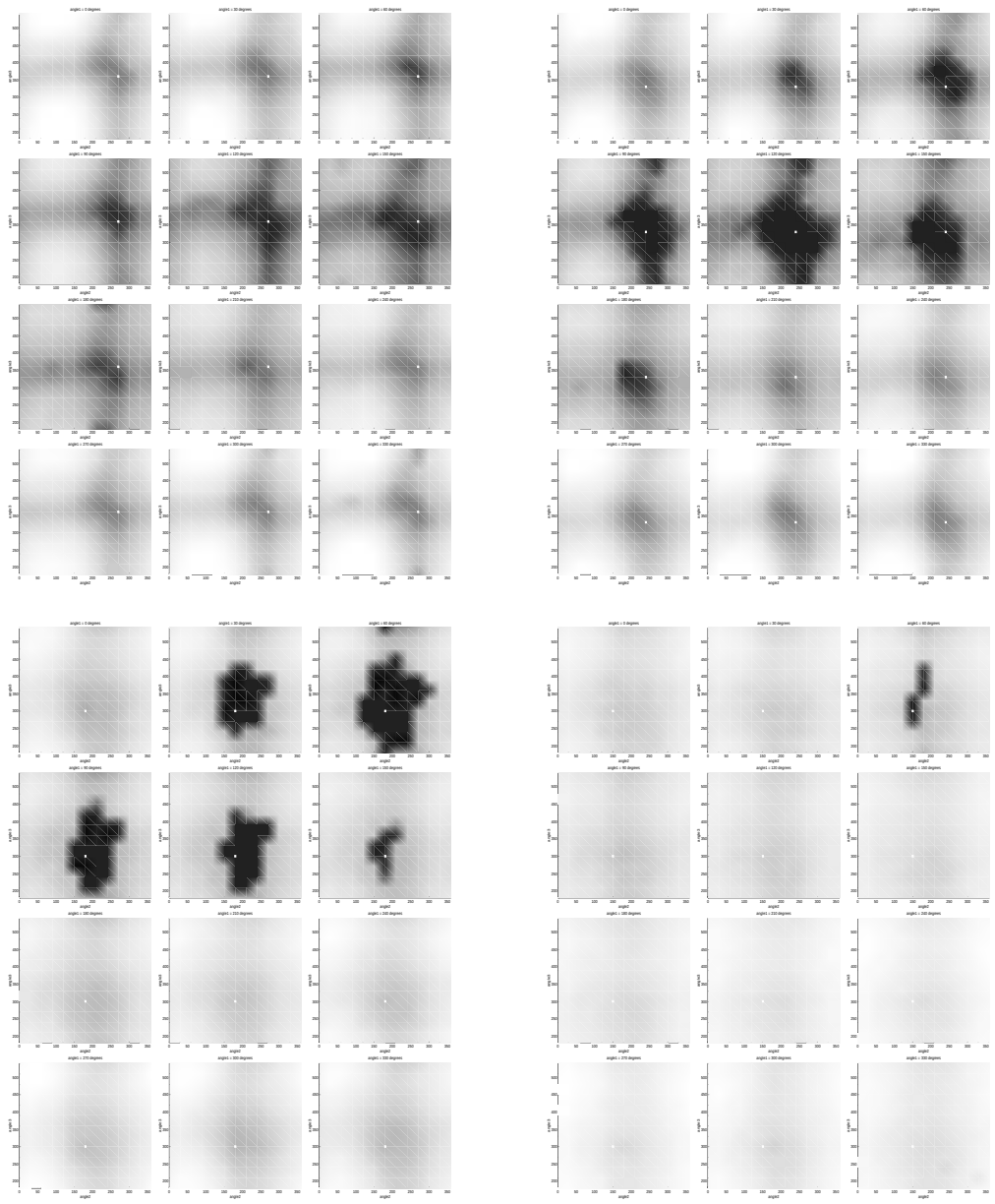

Figure 10: Parametric study, `jeton` = 11,13,17 and 19 (upper left, upper right, lower left, and lower right).

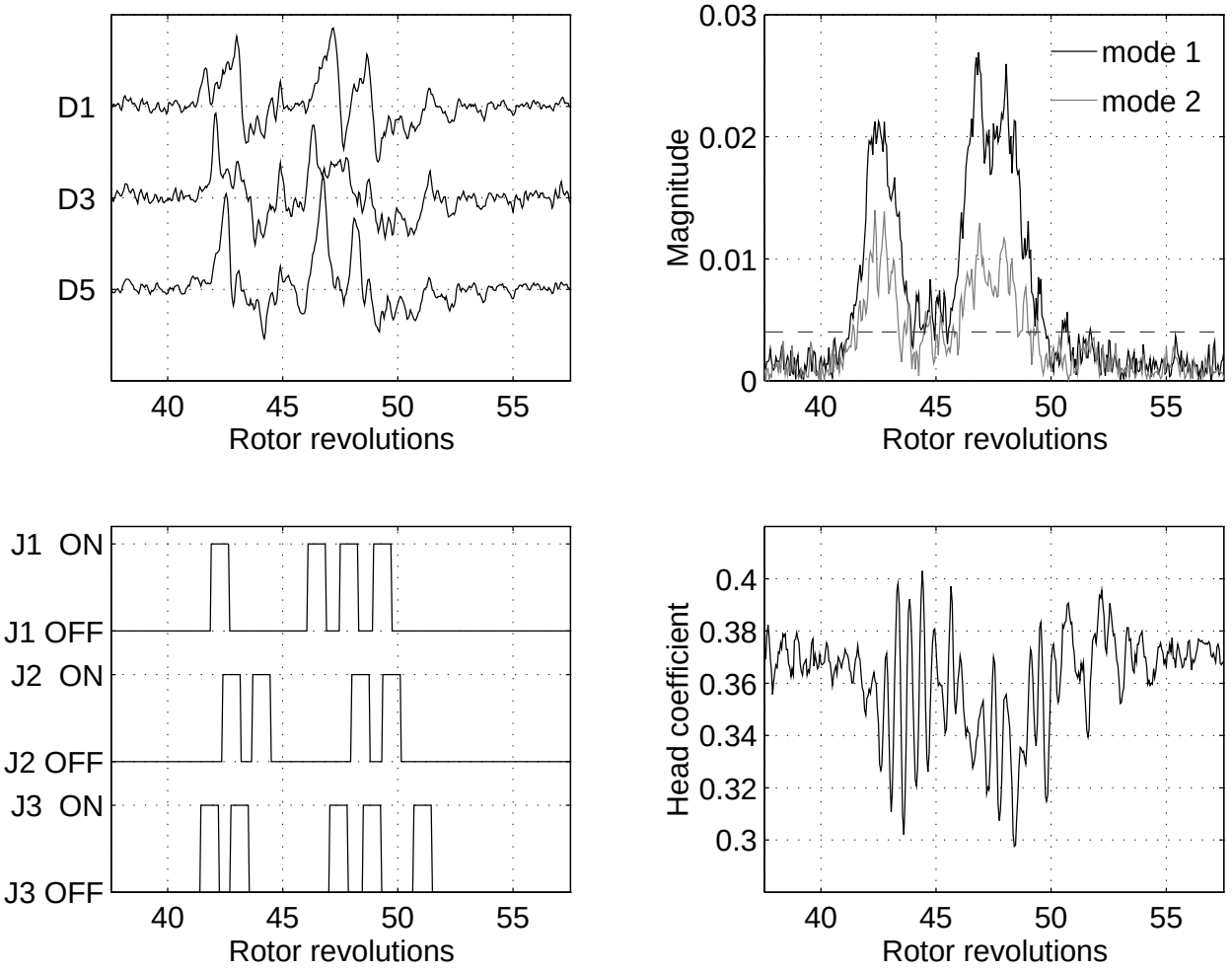


Figure 11: Closed loop operation. The upper left plot consists of the pressure data for transducers 1, 3, and 5. The lower left plot consists of the control signals applied to the air injectors. The upper right plot consists of the calculated first and second mode magnitudes; the dashed line corresponds to the setting for `threshold`. The lower right plot consists of the variation in the head coefficient.

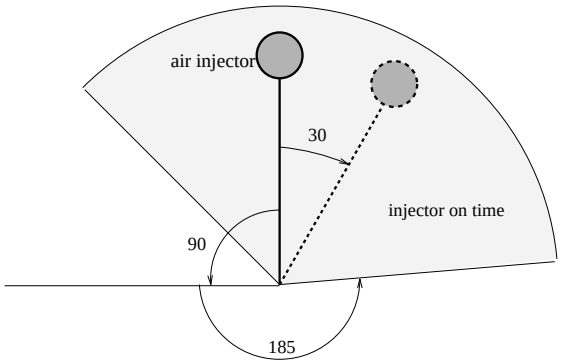


Figure 12: On-time for each air injector. The shaded region corresponds to the location of the peak of the first mode disturbance for which an air injector is on (assuming a constant rotational rate of 65 Hz).

is the unstalled branch, while the other is the stalled branch. If the compressor is unstalled when the air injectors are activated, the operating point will shift to the upper branch; if the compressor is stalled, the operating point will shift to the lower branch (this was verified experimentally). Furthermore, phase information is lost when activating the air injectors for long periods of time. Since there exists a value of `jeton` for which stall is eliminated, it follows that a lower and upper bound exist as well.

The closed loop compressor performance curve is shown in Figure 13 for the optimal choice of injector phasing for `jeton` = 15. The results shown to the left of the peak of the characteristic are time averaged values, since in this region a steady state stall disturbance is present. Error bars are included to show the variation from the mean at these operating points. In general, it was determined that operating points to the left of the peak were not dependent on the initial conditions of the system, ie., the hysteresis region usually associated with stall was eliminated.

### 3.3 Effects of control algorithm on surge dynamics

Several experiments were performed to determine the effect of the control algorithm when the optional plenum was attached to the compressor. The results may be found in Figure 14. At operating point P (see Figure 3), a disturbance lasting 20 rotor revolutions (0.2 seconds) was generated via the high speed bleed valve.

Referring to the uncontrolled data, the system promptly went into surge. As can be seen from the plots, there were two different surge modes, one at 1.4 Hz and the other at 1.8 Hz. The compressor would go into stall during the low pressure rise intervals, and come out of stall during the high pressure rise intervals. The Head coefficient vs. Flow coefficient plot clearly illustrates the surge limit cycle; starting at point P (the asterisk), the graph is traversed in a counter-clockwise direction. The two different surge modes appear as two different closed circuits in this plot, which share a substantial part of the trajectory. Note that the duration of the disturbance corresponded approximately to the time it took for the pressure and flow to reach their minimum value; this observation is important in the analysis of the closed loop behavior below.

Two pressure disturbances were generated approximately 2.5 seconds apart with the controller activated. As before, each pressure disturbance de-stabilized the system. Note that the controller had virtually no effect on the surge trajectory during the time the disturbance was present (in this 20 revolution time period, the trajectory is virtually the same as the one in the previous

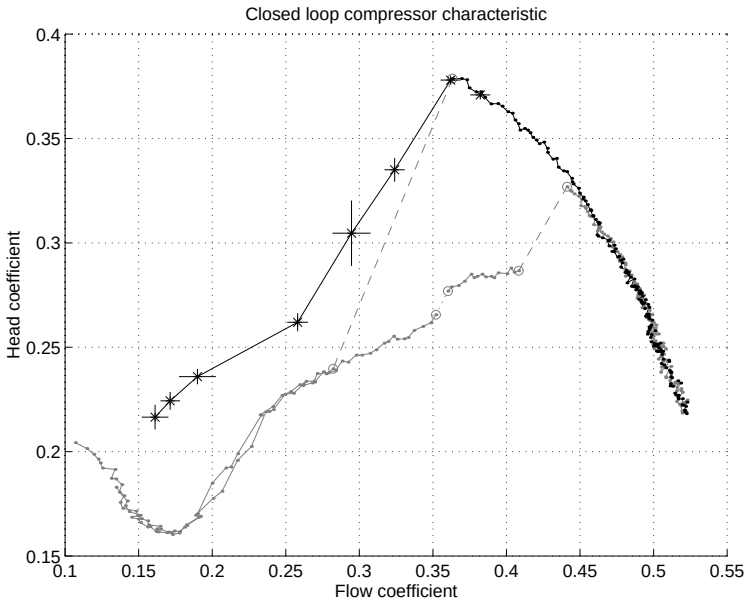


Figure 13: Closed loop compressor characteristic for `jeton` = 15, optimal controller. The asterisks correspond to time averaged data, while the solid lines interpolate these points. The pressure and flow variance are included for each data point as error bars. The open loop compressor characteristic is included for comparison purposes.

experiment). On the subsequent cycle, however, the pressure and flow variations were substantially decreased, and were completely eliminated by the end of the third cycle. It was determined that by shortening the time duration of the pressure disturbance (while still keeping it large enough to cause the open loop system to go into surge), the pressure and flow variations during the first cycle were reduced, with the limiting behavior approaching the trajectories commencing from the second cycle in the plots. Thus if the duration of the disturbance was short enough, the magnitude of the pressure and flow disturbances could be kept to within 30% of the operating pressure and flow.

A possible explanation of why the control algorithm is successful at eliminating stall and surge is the strong coupling between the surge and stall dynamics; the compressor begins to stall when the head coefficient is decreasing. The control algorithm at this point activates, and tries to eliminate the stalled condition. This has the effect of increasing the net pressure rise across the compressor during the periods of decreasing head coefficient. Thus the control algorithm is in effect providing positive damping to the surge dynamics. This is a topic for future research.

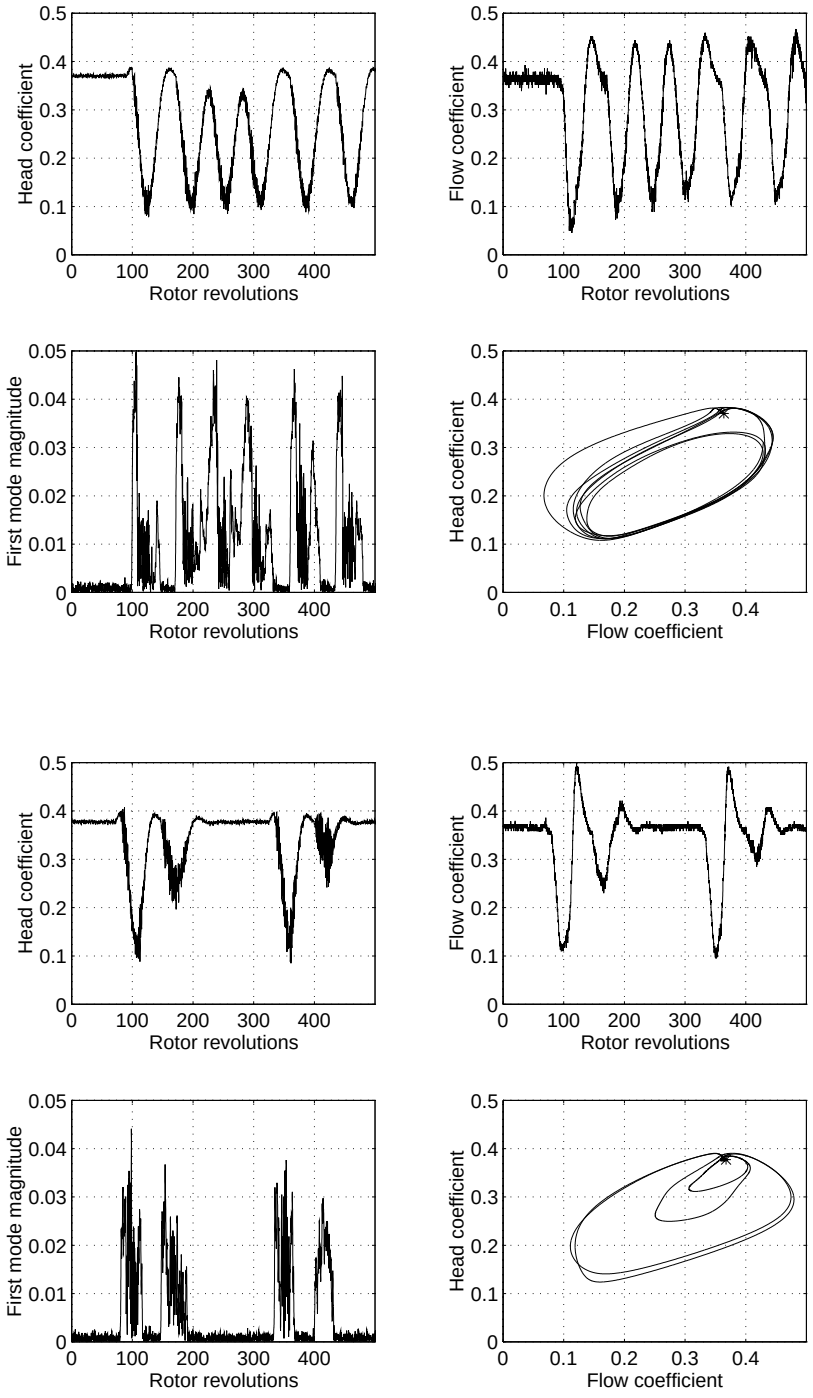


Figure 14: Compressor dynamics with plenum: the top set of plots correspond to data taken without the controller, the bottom set of plots with the controller. All data was low-pass filtered at 150 Hz, except for the Head coefficient vs. Flow coefficient plots, where the data was filtered at 10 Hz; the asterisk in these plots corresponds to operating point P, as per Figure 3.

# 4 Theoretical Validation

In this section, a three state model for a compression system based on a single mode Galerkin projection, proposed by Moore and Greitzer in [23], is used to qualitatively explain the effects of air injection as a stabilizing mechanism. This model is too simple to be able to reproduce in detail the operation of a compressor. In addition, the underlying assumptions include rotational symmetry, which preclude the modeling of air injectors as a localized effect. This model does, however, capture the essential dynamics of the compressor, and allows one to perform symbolic analysis on the system. This in turn will allow us to gain insights into some of the basic properties of our control algorithm.

## 4.1 Moore Greitzer Three State Model

We begin with equations (44), (54), and (55) from [23] which are reproduced here for clarity:

$$\frac{d\bar{\psi}}{d\xi} = \frac{1}{4l_c B^2}\left(\bar{\phi}(\xi) - \gamma\sqrt{\bar{\psi}}\right)$$

$$\frac{1}{2\pi}\int_0^{2\pi} \Psi_c(\bar{\phi} + A\sin\zeta)d\zeta = \bar{\psi} + l_c\frac{d\bar{\phi}}{d\xi} \tag{1}$$

$$\frac{1}{\pi}\int_0^{2\pi} \Psi_c(\bar{\phi} + A\sin\zeta)\sin\zeta d\zeta = \left(m + \frac{1}{a}\right)\frac{dA}{d\xi}.$$

In the equations, $\bar{\psi}$ is the pressure rise coefficient, $\bar{\phi}$ is the annulus averaged flow coefficient, $A$ is the amplitude of the sinusoidal flow coefficient perturbation, $\xi$ is dimensionless time, $\Psi_c$ is the steady state compressor characteristic, and $\gamma$ is the throttle position. The quantities $l_c$, $B$, $a$, and $m$ are parameters which depend on the compression system. For the numerical examples presented later, these parameters which were fit to the Caltech rig.

Based on the experimental results of Section 2, we attempt to model the air injectors as direct actuators of the steady state compressor characteristic, and then analyze the dynamics of the closed loop system when the feedback is proportional to the size of the first mode of the stall cell squared. This does not directly correspond to what was done experimentally, since the phasing information cannot be incorporated into this model. The controlled compressor characteristic is taken to be

$$\Psi_c = \Psi_{cnom} + KA^2\Psi_{cu}, \tag{2}$$

where

$$\Psi_{cnom} = a_0 + a_1\bar{\phi} + a_2\bar{\phi}^2 + a_3\bar{\phi}^3 \qquad \Psi_{cu} = c_0 + c_1\bar{\phi}. \tag{3}$$

By performing the integrals indicated above and substituting $J = A^2$, we obtain the following set of ODEs which describe the dynamics of the compression system:

$$\begin{aligned}
\dot{\bar{\psi}} &= \alpha\left(\bar{\phi} - \gamma\sqrt{\bar{\psi}}\right) \\
\dot{\bar{\phi}} &= \beta\left(\Psi_c - \bar{\psi} + \frac{J}{4}\frac{\partial^2\Psi_c}{\partial\bar{\phi}^2}\right) \\
\dot{J} &= \delta J\left(\frac{\partial\Psi_c}{\partial\bar{\phi}} + \frac{J}{8}\frac{\partial^3\Psi_c}{\partial\bar{\phi}^3}\right),
\end{aligned} \tag{4}$$

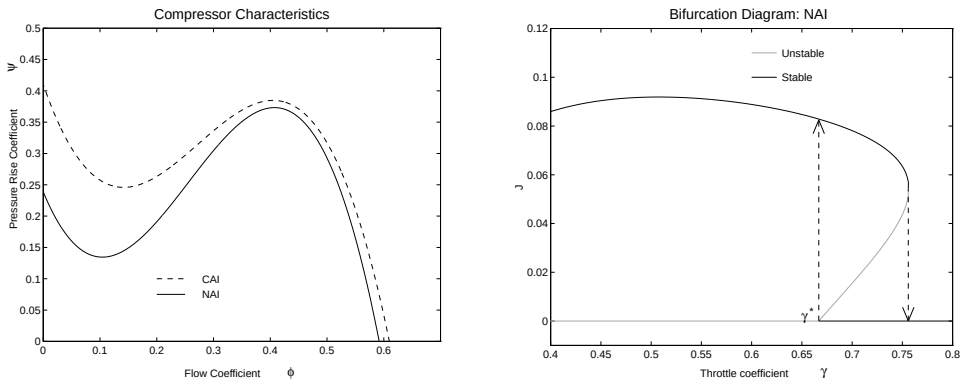


Figure 15: Bifurcation diagram showing jumps associated with the hysteresis loop for the open loop compression system corresponding to the no air injection (NAI) characteristic $\Psi_{\mathrm{cnom}}$ shown at the left. Also shown in the left diagram is the continuous air injection (CAI) shifted characteristic. The linear approximation of the difference between these two characteristics at the stall inception point is $\Psi_{\mathrm{cu}}$.

where

$$\alpha = \frac{1}{4l_cB^2} \qquad \beta = \frac{1}{l_c} \qquad \delta = \frac{2a}{1+ma}. \tag{5}$$

## 4.2 Bifurcation Analysis

The bifurcation properties of the open loop three state compression system model were initially studied by McCaughan [21, 22]. The bifurcations for the pure rotating stall case, the pure surge case, and combination stall/surge case were thoroughly investigated. A throttle based closed loop system for the pure rotating stall case was developed and analyzed by Liaw and Abed [18].

In this paper we are interested only in the pure rotating stall case for the closed loop compression system with the control based on shifting of the steady state compressor characteristic. For the open loop case, the bifurcation diagram for a representative compressor characteristic is known to have a transcritical bifurcation (for the choice of coordinates used in this paper) at the point which corresponds to operating at the peak of the steady state compressor characteristic (see Figure 15). This throttle setting, which corresponds to the peak of the characteristic $(\partial\Psi_c/\partial\bar{\phi}) = 0$, will be denoted by $\gamma^*$. This operating point corresponds to where the stalled branch intersects the horizontal axis in the bifurcation diagram shown in Figure 15.

The unstable sections of the bifurcation diagram in Figure 15 are shown as gray lines, and the stable sections are shown as black lines. This diagram suggests a hysteresis region since as the throttle is closed ($\gamma$ is decreased) $J = 0$ is a stable solution until $\gamma^*$ is reached, at which point the stable solution for $J$ is non-zero (which corresponds to a jump to rotating stall). As $\gamma$ continues to decrease, the stable solution for $J$ continues to be non-zero. If the throttle is then opened, beginning at $\gamma < \gamma^*$, the system continues to evolve along the stalled branch until $\gamma$ is increased to a value substantially greater than $\gamma^*$ before returning to the $J = 0$ branch. The system has substantially different solutions depending on the path that $\gamma$ follows.

We next analyze how the closed loop system based on a shifting of the steady state compressor characteristic effects this bifurcation diagram, and in particular, the hysteresis region. On the

stalled branch of the bifurcation diagram, the following algebraic equations must hold:

$$\bar{\phi}^2 = \gamma^2 \bar{\psi} \tag{6}$$

$$\Psi_c = \bar{\psi} - \frac{J}{4}\frac{\partial^2 \Psi_c}{\partial \bar{\phi}^2} \tag{7}$$

$$\frac{\partial \Psi_c}{\partial \bar{\phi}} = -\frac{J}{8}\frac{\partial^3 \Psi_c}{\partial \bar{\phi}^3}. \tag{8}$$

Since $\bar{\phi}$, $\bar{\psi}$, and $\gamma$ may be determined from $J$ for each equilibrium solution on the stalled branch of the bifurcation diagram, we may differentiate equation (6) with respect to $J$ to obtain

$$2\bar{\phi}\frac{d\bar{\phi}}{dJ} = 2\gamma\frac{d\gamma}{dJ} + \gamma^2\frac{d\bar{\psi}}{dJ}. \tag{9}$$

Differentiating equation (7) with respect to $J$ and evaluating $(d\bar{\psi}/dJ)$ at the peak of the compressor characteristic yields

$$\left.\frac{d\bar{\psi}}{dJ}\right|_{\gamma=\gamma^*} = K\Psi_{cu} + \frac{1}{4}\frac{\partial^2 \Psi_{cnom}}{\partial \bar{\phi}^2}. \tag{10}$$

Similarly, differentiating equation (8) with respect to $J$ yields

$$\left.\frac{d\bar{\phi}}{dJ}\right|_{\gamma=\gamma^*} = \frac{K\dfrac{\partial \Psi_{cu}}{\partial \bar{\phi}} + \dfrac{1}{8}\dfrac{\partial^3 \Psi_{cnom}}{\partial \bar{\phi}^3}}{-\dfrac{\partial^2 \Psi_{cnom}}{\partial \bar{\phi}^2}}. \tag{11}$$

Substituting equations (10) and (11) into equation (9) and solving for $(dJ/d\gamma)$, the slope of the bifurcation diagram at the equilibrium point associated with $\gamma^*$ is:

$$\left.\frac{dJ}{d\gamma}\right|_{\gamma=\gamma^*} = \frac{\sqrt{\bar{\psi}}}{\dfrac{K\dfrac{\partial \Psi_{cu}}{\partial \bar{\phi}} + \dfrac{1}{8}\dfrac{\partial^3 \Psi_{cnom}}{\partial \bar{\phi}^3}}{-\dfrac{\partial^2 \Psi_{cnom}}{\partial \bar{\phi}^2}} - \dfrac{\bar{\phi}}{2\bar{\psi}}\left(K\Psi_{cu} + \dfrac{1}{4}\dfrac{\partial^2 \Psi_{cnom}}{\partial \bar{\phi}^2}\right)}, \tag{12}$$

where all expressions in the right hand side of equation (12) are evaluated at the equilibrium point at the peak of the compressor characteristic.

From this expression it is easy to see how varying the gain on the shifted characteristic affects the slope of the bifurcation diagram at $\gamma^*$. Typically, $(dJ/d\gamma)|_{\gamma=\gamma^*}$ is positive (as is shown in the bifurcation diagram in Figure 15) and if this positive value were increased, the size of the hysteresis region could be decreased. If the shifted portion of the characteristic, $\Psi_{cu}$, has a positive offset term ($c_0 > 0$) the slope will be increased by a positive gain $K$, and if the shifted characteristic has a negative linear term ($c_1 < 0$) the slope will also be increased for a positive gain $K$. Both of these conditions are satisfied for the experimentally determined shifted compressor characteristic. The left plot in Figure 16 shows how the bifurcation diagram changes as the gain $K$ is increased.

This same type of analysis can also be used to show that the hysteresis loop in the bifurcation diagram cannot be changed with nonlinear feedback of $\bar{\psi}$ or $\bar{\phi}$ via throttle control (as was also shown previously in [18]).

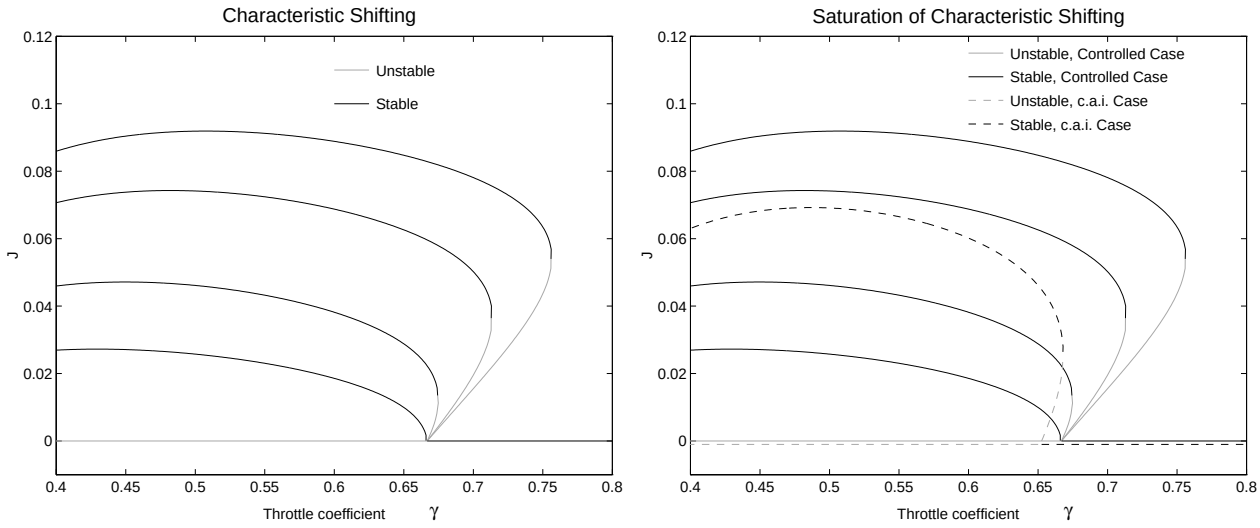


Figure 16: Change in bifurcation diagram as $K$ is varied for the Caltech compressor. The top curve corresponds to $K = 0$. In the right plot, the bifurcation diagram for the CAI case is included to show the saturation limits based on the maximum characteristic shift obtained using air injection on the Caltech rig.

### 4.3 Effects of Saturation

The entire family of bifurcation diagrams shown in the left plot of Figure 16 may not be physically possible in practice; there will be a maximum amount that the steady state compressor characteristic can be shifted. In the right plot, the maximal amount that that the characteristic can be shifted for the air injectors on the Caltech compressor is included. This curve corresponds to the bifurcation diagram generated by the compressor characteristic for the CAI case. This saturation of the actuators translates to a direct limit on how much the closed loop bifurcation diagram can be modified. Shifts which lie to the right of the saturation line are allowed, and for shifts which lie to the left, the saturation line becomes the curve that describes the system behavior.

Based on the previous analysis, the amount of characteristic shifting required to eliminate the rotating stall hysteresis loop would be the amount for which equation (12) is infinite. In practice this calculation may be conservative. In most applications, noise will drive the compressor into rotating stall at a value of $\gamma$ which is substantially greater than $\gamma^*$. This throttle position will therefore dictate the amount that the characteristic must be shifted in order to eliminate the hysteresis loop.

It is clear that the above analysis does not completely explain the experimental results shown in Figure 13, since the hysteresis region is not eliminated. This is expected, since phasing information is not included in the above analysis. This analysis is in agreement, however, with the control algorithm configured to turn all the air injectors on at once when a stall disturbance was sensed; it was experimentally determined that this strategy was not successful at eliminating the hysteresis region. What the above analysis provides is some guidelines on what types of shifts of the characteristic are desirable, and provides an upper bound on the amount of shifting required to eliminate the hysteresis region.

# 5 Simulations

In this section, simulations using a higher fidelity model are presented which overcome some of the limitations of the analysis performed on the three state model. The model used here is the distributed model of Mansoux et al. [20], and is a system of equations describing the dynamics of the flow coefficient $\phi$ at discrete points around the compressor annulus. The simulations presented here also include additional effects such time lags associated with change in the pressure rise delivered ($\Psi_c(\phi)$ has dynamics associated with it) and the mass/momentum addition effects associated with air injection. The model is attractive because the steady state compressor characteristic shifting can be included in a local way instead of as an axially averaged shift (as was done in the previous analysis), and thus the compressor characteristic can be shifted in phase as well as in magnitude. The distributed model was used to perform a simulation based parametric study similarly to what is was performed on the experiment and to model the hysteresis regions of compressor running with and without the air injection. We first present the equations of the basic distributed model and then describe simulation results.

## 5.1 Distributed Model

The full details of the distributed model presented in Mansoux et al. [20] should be obtained from that reference; only the details required to explain how the compressor characteristic shifting was included in the model will be presented here. The final equations (equation (20)) from [20] which make up the distributed model for a compression system are given by:

$$\dot{\bar{\psi}} = \frac{1}{4l_c B^2}\left(S\phi - \gamma\sqrt{\bar{\psi}}\right) \tag{13}$$

and

$$G^{-1}D_E G\dot{\phi} = -G^{-1}D_A G\phi + \Psi_c(\phi) - T\bar{\psi} \tag{14}$$

where $\bar{\psi}$ is the annulus averaged pressure rise coefficient, $\phi$ is the vector of flow coefficients at discrete points around the compressor annulus, $\gamma$ is the throttle position, and $D_A$, $D_E$, $T$, $S$, $B$ and $l_c$ are constants which depend on the compressor rig (see [20]). $G$ is the discrete Fourier transform matrix, i.e.

$$\phi = \begin{bmatrix} \phi_1 \\ \phi_2 \\ \vdots \\ \phi_{2n+1} \end{bmatrix} \qquad G : \phi \mapsto \begin{bmatrix} \tilde{\phi}_0 \\ \text{Re } \tilde{\phi}_1 \\ \text{Im } \tilde{\phi}_1 \\ \vdots \\ \text{Re } \tilde{\phi}_n \\ \text{Im } \tilde{\phi}_n \end{bmatrix}$$

where $\tilde{\phi}_i$ is the Fourier coefficient associated with mode $i$ and $n$ is the number of modes included in the model. Seven modes were used for the results presented in this paper. Two additional effects not included in the above equations but included in the simulations presented here are the effects of unsteady flow on the pressure rise delivered by the compressor and the mass/momentum addition terms associated with air injection. The unsteady flow effects on the delivered pressure rise have been studied by Haynes et al. [15], and the linear model presented there is straightforward to append to the dynamics reproduced here (this is suggested in the distributed model presentation in [20]). The mass/momentum addition terms associated with the air injection were derived for the linear case by Hendricks and Gysling in [16]. The results presented there have been extended

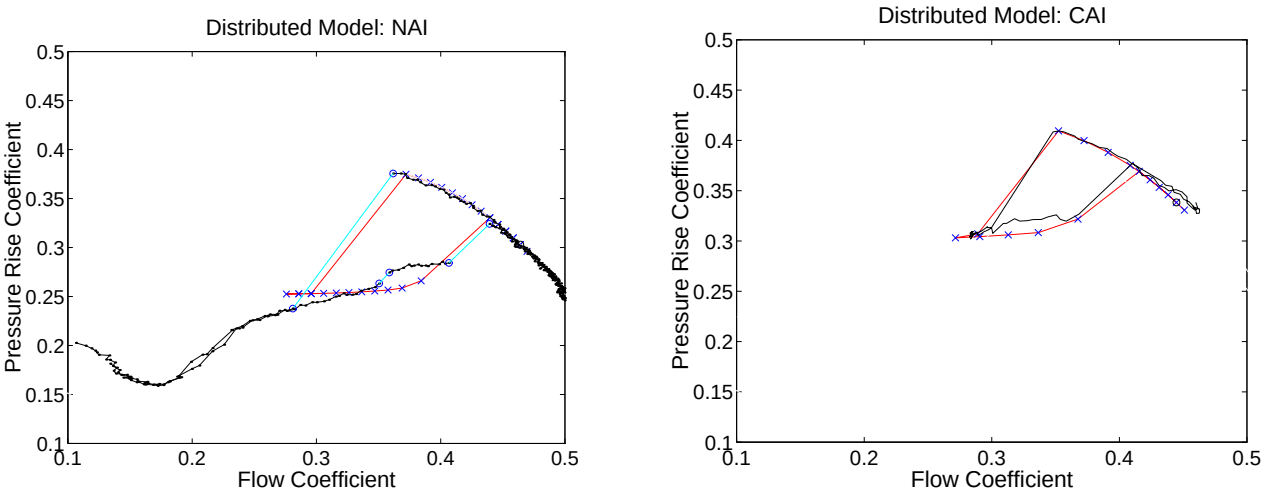


Figure 17: Hysteresis loops for simulation compressor characteristics. The left plot corresponds to the fit for the NAI case, the right plot corresponds to the fit for the CAI case. Simulation data points are denoted with an `x`.

to include the nonlinear terms for the simulations presented here. A complete description of our modeling efforts is beyond the scope of this paper, for additional details see [4].

The Caltech compressor rig has three air injectors placed 120 degrees apart around the compressor annulus (as in Figure 2), and each injector has an effect on a small region of the compressor rotor. In the distributed model, the vector of pressure rise coefficients around the compressor annulus is given by $\Psi_c$. In order to include the compressor characteristic shifting as a local effect, the shift is included as

$$\Psi_c(\phi_i) = \Psi_{cnom}(\phi_i) + (\Psi_{csh}(\phi_i) - \Psi_{cnom}(\phi_i))\, L(u_i) \tag{15}$$

at the three points around the annulus which have injectors associated with them and as

$$\Psi_c(\phi_i) = \Psi_{cnom}(\phi_i) \tag{16}$$

for the remaining positions. Here $\Psi_{cnom}$ is the nominal compressor characteristic, while $\Psi_{csh}$ is the locally shifted characteristic. The control variables are the $u_i$, which take the values of 0 or 1 if the air injector is off or on respectively. The transient effect of the air injection on the compressor characteristic shift is modeled as a delay followed by a first order lag; this is captured by operator $L$. The values for the delay and lag were chosen to correspond to the values observed in the experiment.

The geometric parameters associated with the distributed model were first calculated from physical measurements of the Caltech rig, and initial guesses were taken for those that remained. The simulation parameters were then adjusted (specifically the compressor characteristics) to match the rotation and growth rate of the transition to rotating stall and to match the pressure rise delivered during fully developed rotating stall. Compressor characteristics were determined for both the no air injection (NAI) and continuous air injection (CAI) cases, as per the experimental data shown in Figure 5. Figure 17 shows the compressor characteristics used in simulation for both cases, as well as the experimental data for comparison purposes.

Since the simulation parametric study will compare how controllers respond to a disturbance from the peak of the unstalled compressor characteristic (as was done for the experimental setup),

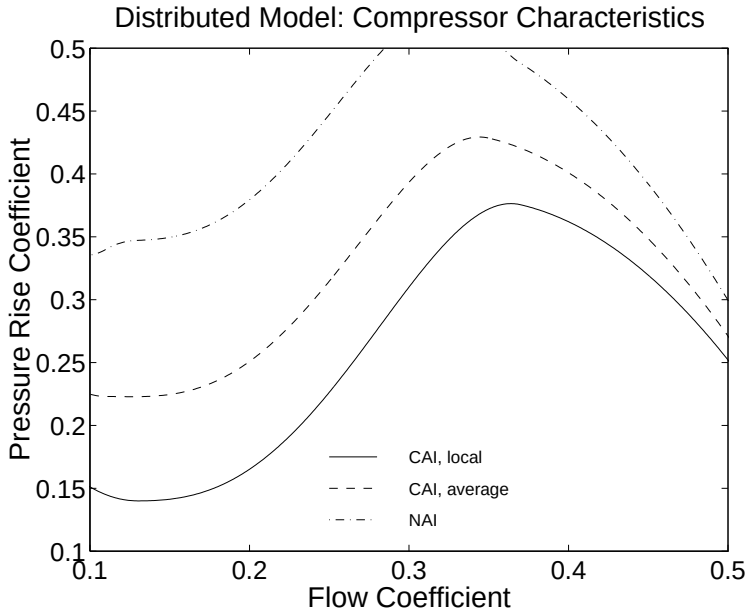


Figure 18: Shifted compressor characteristics.

the compressor characteristics for the two cases were selected so that stall occurred at the same point as determined experimentally (there is a slight discrepancy to account for the noise in the experimental setup). In addition, the characteristics were adjusted so that the open loop simulations corresponded to the behavior observed experimentally at the transition to stall and at recovery from rotating stall. For this reason, the simulated open loop characteristics do not match up perfectly with those observed experimentally over the entire hysteresis region. In order to correct these errors, the details of fully developed rotating stall would have to be modeled over the entire range of the throttle settings, and a substantially more complicated model would be required.

The next step was to simulate the open loop air injection case with a non-uniform compressor characteristic. From the characteristics shown in Figure 17, the equivalent local compressor characteristic for the stations where air injectors are located, $\Psi_{\mathrm{csh}}$, can be determined. This was done by requiring that the average characteristic obtained when using the characteristic shown on the right of Figure 17 have the same value as that obtained when using the locally shifted characteristic at three stations, and the average nominal compressor characteristic (shown on the left in Figure 17) at the remaining stations. The plot on the left of Figure 18 shows the characteristics used in the simulation study, and the plot on the right shows the resulting hysteresis loop obtained via simulation using the local non-uniform characteristic.

## 5.2 Parametric Study

The goal of the simulation based parametric study was to determine the optimal control strategy based on a model for the compressor. In particular, a search for the optimal phasing for the activation of each air injector relative to the measured position of the peak of the first mode stall disturbance was performed.

The control algorithm was essentially the same as the one described in Figure 7 in Section 3. The major difference was in the implementation of what corresponded to activating the air injectors for `jeton` number of servo iterations in the experimental study. This was accomplished by activating

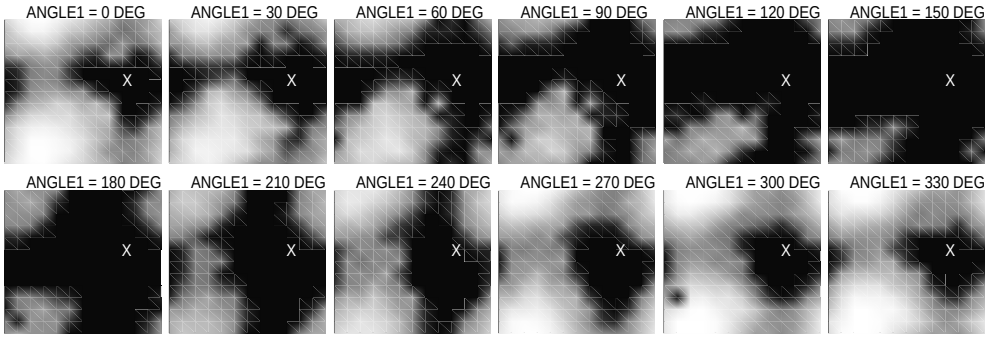


Figure 19: Simulation parametric study. Dark areas correspond to low average values for the first mode disturbance, light areas correspond to large average values. The horizontal axis for each plot corresponds to `angle2`, $0 - 360$ degrees; the vertical axis corresponds to `angle3`, $180 - 540$ degrees, shifted to center the dark areas. The white 'X' corresponds to the optimal setting for `angle2` and `angle3`

each air injector when the magnitude of the first mode disturbance became greater than some threshold magnitude and the phase of the first mode disturbance was within a pre-specified window. The threshold magnitude was based on the noise level in the experimental determination of the magnitude of the first mode.

In terms of the logic of Figure 7, this corresponds to setting `jeton` to 0 and `window` to 120 degrees, and running the servo loop at an infinitely high rate. This is roughly how the control algorithm behaved in the experimental studies. This algorithm was used to simplify the simulation code and vastly decrease its running time.

As in the experimental study, the phasing of each air injector was independently varied in 30 degree increments. For each controller tested, the average amplitude of the first mode stall cell was recorded. In all the simulations, the same initial stall cell disturbance (both in magnitude and phase) was used. Analogously to the experimental results of Figure 8, the simulation results are shown in Figure 19. The simulation study predicts the same periodic trends for the optimal phasing as are seen in the experimental data.

The optimal phase setting for the simulation parametric study is approximately (150, 270, 30). The activation, de-activation, and transport delays were implemented by a Pade approximation. In the experimental setup, the air injectors were not symmetric with respect to the turn on and turn off times; it was found that the air injectors would take approximately 2 ms longer to turn on than to turn off (this was taken into account in the analysis of Figure 12), which corresponds to roughly 50 degree of stall rotation. This asymmetry was not implemented in the simulation. When this 50 degree lead is subtracted from the above optimal setting, a value consistent with the optimal setting obtained experimentally is obtained.

### 5.3 Closed Loop Simulations

The closed loop characteristic for the optimal controller obtained via simulation is shown in Figure 20. The hysteresis region has essentially been eliminated, as was determined experimentally. The transition to rotating stall is also gradual, i.e. there is no jump from zero stall to fully developed stall. These two results, along with the matching of the trends between the experimental and simulation parametric studies strongly support the air injection model presented here. Further

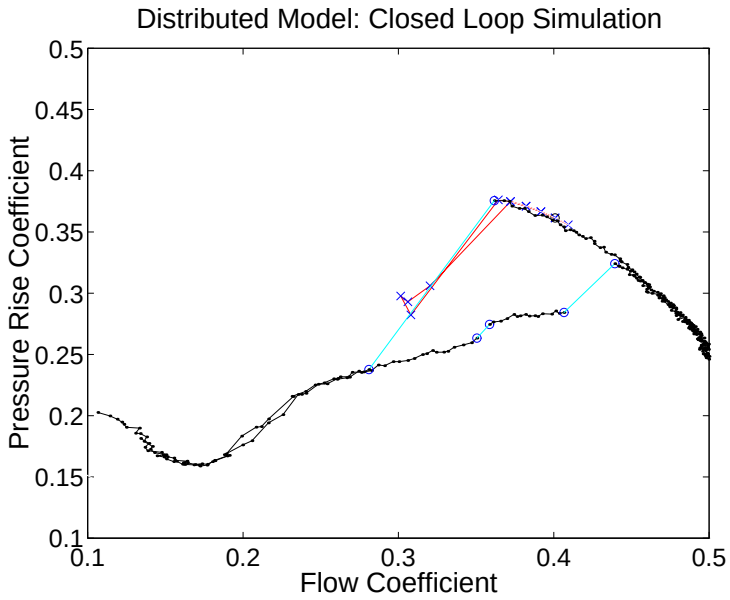


Figure 20: Simulated closed loop compressor characteristic. Simulation data points are denoted with an `x`.

work on refining the model will focus on using numerical techniques to determine the bifurcation characteristics, and coupling surge controllers with the pulsed air injection controller for rotating stall.

# 6 Conclusions and Future Work

The active control techniques developed in this paper proved to be simple, easy to implement, yet at the same time extremely effective in eliminating the hysteresis region normally associated with stall. The analytical study performed on the Moore-Greitzer three state model qualitatively supports the experimental results obtained, and explains the basic bifurcation behavior of the closed loop system. Furthermore, the simulation studies performed with a higher fidelity model were in agreement with the experimental results, and justified the modeling of air injection as a localized shift in the compressor characteristic.

The main physical phenomenon which was utilized in the experimental work and the ensuing analysis was that the steady state compressor characteristic could be shifted by injecting air at the face of the compressor. While it has been previously shown that by introducing pre-swirl at the inlet and by the use of inlet guide vanes the compressor characteristic can be altered for many compressors [19], the extent to which this effect can be achieved using air injection is an open research topic. The impact of the results in this paper thus hinge on demonstrating the genericness of shifting the compressor characteristic using localized air injection.

The experiments were performed with three air injectors at a fixed flow rate and distance from the compressor face. It is important to characterize how the performance of the control design varies by varying these parameters. For example, given an upper limit on the total flow which can be introduced by the air injectors, what is the optimal number of air injectors which should be used for feedback control? How should they be oriented relative to the compressor face? What is the tradeoff between the velocity of injected air and the performance of the compressor? These same questions can be asked for a fixed power limit on the actuation, or velocity limit, or combinations thereof. In order to answer these questions, more parametric studies need to be performed, and a more detailed model which captures the fluid dynamical interactions needs to be developed and studied.

While it is important to determine how the closed loop performance varies as a function of these parameters, it is equally important to determine the regions of implementability for these parameters. For example, injecting air at a velocity which is much greater than the mean velocity through the compressor would not be feasible for high speed systems. It is also desirable to use recirculation as the means to provide the needed flow for air injection [14], which will restrict the velocity at which air can be injected. Another issue is the effect of pulsing high momentum flow onto the rotor blades; this should be studied to determine what the detrimental effects are, and see if they are offset by the resulting benefits.

Even though controlling stall was the main purpose of the work presented in this paper, the elimination of surge is also an important aspect of extending the operability of a compressor. We have demonstrated that the controller designed to control stall can also have positive effects in eliminating surge. This is mainly due to the strong coupling between surge and stall, although a more detailed analysis needs to be performed to fully determine this interaction. Furthermore, the transients which occur when stabilizing surge need to be made as small as possible in order to prevent the compression system from being damaged. One of our future research goals is to incorporate bleed valve control with pulsed air injection to simultaneously control surge and stall, and minimize these transient effects.

## Acknowledgements

The authors would like to thank Simon Yeung, Wayne Hurwitz, Jim Paduano, Carl Nett, Kevin Eveker, Dan Gysling, Allan Acosta, and John Doyle for their many helpful suggestions and comments.

## References

[1] E. H. Abed, P. K. Houpt, and W. M. Hosny. Bifurcation analysis of surge and rotating stall in axial flow compressors. *Journal of Turbomachinery*, 115:817–824, October 1993.

[2] AMCA/ASHRAE. Laboratory methods of testing fans for rating. Technical Report ANSI/AMCA Standard 210-85, Air Movement and Control Association, 1985.

[3] O. O. Badmus, S. Chowdhury, K. M. Eveker, and C. N. Nett. Control-oriented high-frequency turbomachinery modeling - single-stage compression system one-dimensional model. *Journal of Turbomachinery*, 117:47–61, January 1995.

[4] R. L. Behnken. *Nonlinear Control and Modeling of an Axial Flow Compressor*. PhD thesis, Department of Mechanical Engineering, California Institute of Technology, 1997.

[5] R. L. Behnken, R. D'Andrea, and R. M. Murray. Control of rotating stall in a low-speed axial flow compressor using pulsed air injection: Modeling, simulations, and experimental validation. In *Proc. IEEE Control and Decision Conference*, pages 3056–3061, 1995.

[6] R. D'Andrea, R. L. Behnken, and R. M. Murray. Active control of rotating stall using pulsed air injection: A parametric study on a low-speed, axial flow compressor. In *Sensing, Actuation, and Control in Aeropropulsion; SPIE International Symposium on Aerospace/Defense Sensing and Dual-Use Photonics*, pages 152–165, 1995.

[7] I. J. Day. Active supression of rotating stall and surge in axial compressors. *Journal of Turbomachinery*, 115:40–47, 1993.

[8] I. J. Day. Stall inception in axial flow compressors. *Journal of Turbomachinery*, 115:1–9, 1993.

[9] K. M. Eveker, D. L. Gysling, C. N. Nett, and O. P. Sharma. Integrated control of rotating stall and surge in aeroengines. In *Sensing, Actuation, and Control in Aeropropulsion; SPIE 1995 International Symposium on Aerospace/Defense Sensing and Dual-Use Photonics*, pages 21–35, 1995.

[10] G. B. Gilyard and J. S. Orme. Subsonic flight test evaluation of a performance seeking control algorithm on an F-15 airplane. In *Joint Propulsion Conference and Exhibit*, pages AIAA paper 92–3743, 1992.

[11] E. M. Greitzer. Surge and rotating stall in axial flow compressors—Part I: Theoretical compression system model. *Journal of Engineering for Power*, pages 190–198, April 1976.

[12] E. M. Greitzer. The stability of pumping systems—The 1980 Freeman scholar lecture. *ASME Journal of Fluids Engineering*, 103:193–242, 1981.

[13] D. L. Gysling. *Dynamic Control of Rotating Stall in Axial Flow Compressors Using Aeromechanical Feedback*. PhD thesis, Department of Aeronautics and Astronautics, Massachusetts Institute of Technology, Cambridge, Massachusetts, 1993.

[14] D. L. Gysling and E. M. Greitzer. Dynamic control of rotating stall in axial-flow compressors using aeromechanical feedback. *Journal of Turbomachinery*, 117(3):307–319, 1995.

[15] J. M. Haynes, G. J. Hendricks, and A. H. Epstein. Active stabilization of rotating stall in a three-stage axial compressor. *Journal of Turbomachinery*, 116:226–239, 1994.

[16] G. J. Hendricks and D. L. Gysling. Theoretical study of sensor-actuator schemes for rotating stall control. *Journal of Propulsion and Power*, 10(1):101–109, 1994.

[17] A. Khalak and R. M. Murray. Experimental evaluation of air injection for actuation of rotating stall in a low speed, axial fan. In *Proc. ASME Turbo Expo*, 1995.

[18] D. C. Liaw and E. H. Abed. Active control of compressor stall inception: A bifurcation-theoretic approach. Technical report, Institute for Systems Research, Univ. of Maryland, 1992. Also appears in Proceedings of NOLCOS '92 , M. Fliess, ed., Pergammon Press.

[19] J. P. Longley. A review of nonsteady flow models for compressor stability. *Journal of Turbomachinery*, 116:202–215, 1994.

[20] C. A. Mansoux, D. L. Gysling, J. D. Setiawan, and J. D. Paduano. Distributed nonlinear modeling and stability analysis of axial compressor stall and surge. In *Proc. American Control Conference*, pages 2305–2316, 1994.

[21] F. E. McCaughan. Application of bifurcation theory to axial flow compressor instability. *Journal of Turbomachinery*, 111:426–433, 1989.

[22] F. E. McCaughan. Bifurcation analysis of axial flow compressor stability. *SIAM Journal of Applied Mathematics*, 20(5):1232–1253, 1990.

[23] F. K. Moore and E. M. Greitzer. A theory of post-stall transients in axial compression systems—Part I: Development of equations. *Journal of Turbomachinery*, 108:68–76, 1986.

[24] J. D. Paduano, A. H. Epstein, L. Valavani, J. P. Longley, E. M. Greitzer, and G. R. Guenette. Active control of rotating stall in a low-speed axial compressor. *Journal of Turbomachinery*, 115:48–56, January 1993.

[25] J. D. Paduano, E. M. Greitzer, A. H. Epstein, G. R. Guenette, D. L. Gysling, J. Haynes, G. J. Hendricks, J. S. Simon, and L. Valavani. Smart engines: Concept and application. *Integrated Computer-Aided Engineering*, 1(1):3–28, 1993.

[26] R. H. Smith, J. D. Chisholm, and J. F. Stewart. Optimizing aircraft performance with adaptive, integrated flight/propulsion control. *Journal of Engineering for Gas Turbines and Power*, 113(87–94), 1991.